Chapter 6

# Holographic Data Storage Using Parallel-Aligned Liquid Crystal on Silicon Displays

Francisco J. Martínez Guardiola,
Andrés Márquez Ruiz, Sergi Gallego Rico,
Roberto Fernández Fernández,
Jorge Francés Monllor, Manuel Ortuño Sánchez,
Inmaculada Pascual Villalobos and
Augusto Beléndez Vázquez

Additional information is available at the end of the chapter

http://dx.doi.org/10.5772/67158

**Abstract**

The parallel-aligned liquid crystal on silicon (PA-LCoS) microdisplay has become a widely used device for the photonics community. It is a very versatile tool that can perform several tasks which transforms it into a key element in many different photonics applications. Since our group is interested in holography, in this chapter, we want to use these displays as the data entry point for a holographic data storage system (HDSS). Due to the novelty of this kind of device, we have done an intense work characterizing it. These efforts are reflected in this chapter where the reader will find two different characterization methods that will enable to predict the performance of the device in a specific application. Additionally, we present how a phase-only device can be used as a data pager using different modulation schemes and combined with a photopolymer as the holographic recording material.

**Keywords:** holographic data storage, PA-LCoS, modulation schemes, liquid crystal, photopolymer

## 1. Introduction

In this chapter, we present an analysis on the use of modern parallel-aligned liquid crystal on silicon displays (PA-LCoS) in diffractive optics and holographic data storage (HDS). The PA-LCoS acts as a spatial light modulator (SLM) in different roles: as data entry point,

state of polarization (SOP) converter, phase-only modulator, or amplitude-mostly modulator. All these roles are interesting in many research fields [1–3].

PA-LCoS devices have become widely used in diffractive optics due to its ease of operation and phase-only modulation capabilities, because of its high spatial resolution and high light efficiency [3]. The liquid crystal (LC) technology has achieved a high level of maturity and enables us to have a data entry point in HDS for a high data density recording, and it provides us with the ability to design different modulation schemes.

In order to incorporate this kind of microdisplays into a complete holographic data storage system (HDSS), we have done an intense work to characterize PA-LCoS devices. As a phase-only device, we need to know the retardance introduced for every gray level. The microdisplay is digitally addressed with a pulsed voltage signal. This fact implies a fluctuation in the phase that will be reflected in the optical response [4–7]. For that reason, for a full characterization, we need to obtain the average retardance and the fluctuation amplitude for every gray level. This enables us to select the best device configuration for our application.

Even though PA-LCoS are widely used by the photonics community, these phase-only devices have not been intensively applied in holographic data storage applications. These devices could be a key element for a phase multilevel data page coding. If the trend is to use this kind of coding scheme, a right characterization and a profound knowledge will be useful.

## 2. PA-LCoS characterization

In this section, we present two characterization methods for PA-LCoS microdisplays. One of them uses any equipment that is present in almost every optics laboratory. The other makes use of a commercial rotating wave plate polarimeter.

### 2.1. Extending the linear polarimetric method to characterize the PA-LCoS

Parallel-aligned devices are totally characterized by their linear retardance versus voltage values. For this reason, we can use methods typically used in the characterization of wave plates. All these methods assume that the retardance introduced does not change with time [8, 9]. So, we have to adapt the method for elements that present some levels of fluctuation in the retardance signal.

We use the linear polarimetric method to measure the retardance introduced by the wave plate (our PA-LCoS). We use the next scheme.

In **Figure 1**, we see a wave plate sandwiched between two linear polarizers. For the appropriate angles between wave plate and the linear polarizers, we can calculate the retardance as follows [7]:

$$\Gamma = \cos^{-1}\left(\frac{I^{//}_{OUT} - I^{\perp}_{OUT}}{I^{//}_{OUT} + I^{\perp}_{OUT}}\right) \quad (1)$$

http://dx.doi.org/10.5772/67158

where $\Gamma$ is the measured retardance. $I_{OUT}^{\parallel}$ and $I_{OUT}^{\perp}$ are the intensity measured at the exit of the system when the two linear polarizers are oriented at +45° with respect to the slow axis of the wave plate, and when the input linear polarizer is oriented at +45° and the output polarizer is oriented at −45°. These are the so-called "parallel" intensity and "crossed" intensity. With just two measurements, we can calculate the retardance of the wave plate. These intensities are defined as follows:

$$I_{OUT}^{//} = \frac{I_0}{2}[1+\cos\Gamma] \tag{2}$$

$$I_{OUT}^{\perp} = \frac{I_0}{2}[1-\cos\Gamma] \tag{3}$$

where $I_0$ is the total light intensity introduced in the system.

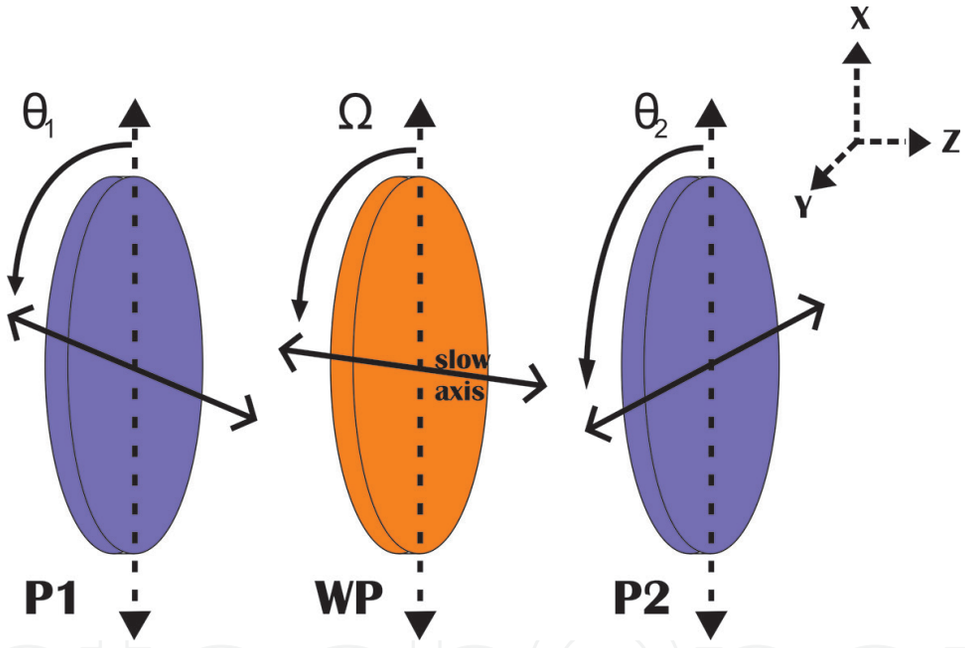


**Figure 1.** Linear polarimeter with the wave plate (WP) to be measured. P1 and P2 are linear polarizers.

As mentioned, the PA-LCoS device introduces a fluctuation due to its digital-addressing scheme. We see how this fact alters the equations described above. As a first approximation, we consider a triangular profile for the periodic variation of retardance with time, $\Gamma(t)$ described by Eq. (4)

$$\Gamma(t) = \begin{cases} \overline{\Gamma} - a + \frac{2a}{T/2}t & 0 \le t < T/2 \\ \overline{\Gamma} + 3a - \frac{2a}{T/2}t & T/2 \le t < T \end{cases} \tag{4}$$

where $\bar{\Gamma}$ is the average value of the retardance during a period $T$. This function is represented in **Figure 2**.

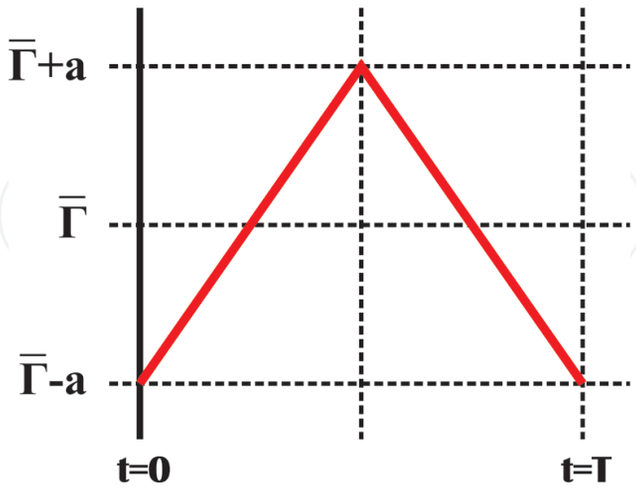


**Figure 2.** Triangular profile considered for the temporal fluctuation of the linear retardance.

Following the proposed model in Eq. (4), if we calculate the average value for a period of $\cos(\Gamma(t))$, we obtain,

$$\left\langle \cos\left(\bar{\Gamma} - a + \frac{2a}{T/2}\, t\right)\right\rangle = \frac{\sin(a)}{a}\cos(\bar{\Gamma}) \tag{5}$$

We can see how a *sinc* term appears modulating the cosine function. Taking into account Eq. (5), we can rewrite Eqs. (2) and (3) in terms of average intensity as follows:

$$\langle I^{//}_{\mathrm{OUT}}\rangle = \frac{I_0}{2}\left[1 + \frac{\sin a}{a}\cos\bar{\Gamma}\right] \tag{6}$$

$$\langle I^{\perp}_{\mathrm{OUT}}\rangle = \frac{I_0}{2}\left[1 - \frac{\sin a}{a}\cos\bar{\Gamma}\right] \tag{7}$$

We see how the intensity that we really measure is affected by the *sinc(a)* function when we are trying to measure the retardance introduced by a wave plate that presents instabilities. If we combine Eqs. (6) and (7), we obtain the next expression for the average retardance:

$$\frac{\langle I^{//}_{\mathrm{OUT}}\rangle - \langle I^{\perp}_{\mathrm{OUT}}\rangle}{\langle I^{//}_{\mathrm{OUT}}\rangle + \langle I^{\perp}_{\mathrm{OUT}}\rangle} = \frac{\sin a}{a}\cos\bar{\Gamma} \tag{8}$$

$$\bar{\Gamma} = \cos^{-1}\left(\frac{\left(\langle I^{//}_{\mathrm{OUT}}\rangle - \langle I^{\perp}_{\mathrm{OUT}}\rangle\right)/\left(\langle I^{//}_{\mathrm{OUT}}\rangle + \langle I^{\perp}_{\mathrm{OUT}}\rangle\right)}{\left(\sin a/a\right)}\right) \tag{9}$$

In the case when no fluctuation exist ($a = 0^{\circ}$), we recover the classical result presented in Eq. (1). In essence, assuming a linear variation with time, as expressed in Eq. (4), this fluctuation is translated into a *sinc* function when averaging the cosine in a period.

http://dx.doi.org/10.5772/67158

To analyze how the fluctuations limit the classical linear polarimeter, we performed the next simulated experiment: using Eqs. (6) and (7), we simulate the intensity values measured in the presence of fluctuations in the retardance. Then, we consider Eq. (1) to obtain the retardance value as if we ignore the existence of these fluctuations.

In **Figure 3**, we show the calculated retardance values as a function of the true retardance ones used in the simulation and for different fluctuation amplitudes, indicated with the curves in the plot.

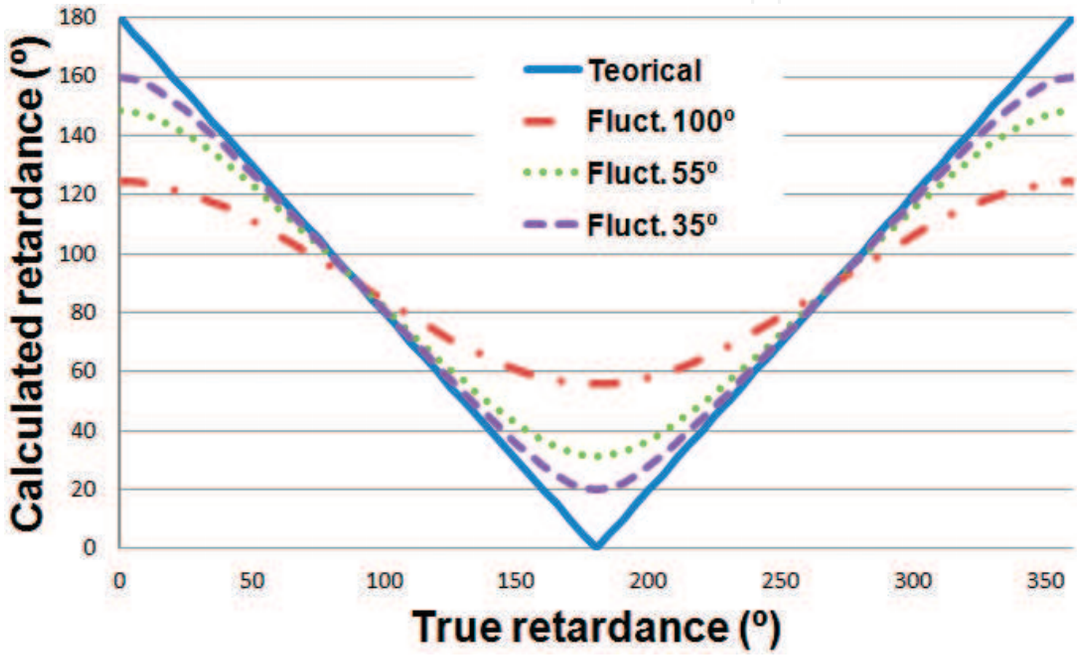


**Figure 3.** Simulation of the retardance measurement experiment in the presence of fluctuations. The calculated retardance uses the classical expression where fluctuations are not considered. Various fluctuation amplitudes are considered to be compared with the no-fluctuations case.

In **Figure 3**, we see how the fluctuations affect the calculated retardance. The maximum and the minimum measurements are produced at the same places of the theoretical wrapped retardance. This means that they are produced at values multiple of 180°. We also note that the deviation amount of deviation depends on the true retardance value. At true retardance, values multiple of 180° deviation are magnified. Outside of these points, if the fluctuation amplitude is not very large, we also find that the calculated values are very close to the true retardance values.

From the study of Eq. (8), it can be easily deduced that for average retardance values multiple of 180°, the calculated retardance only depends on the fluctuation amplitude $a$. So, in these cases we can uncouple the average retardance measurements from the fluctuation amplitude. These cases are the maximum and minimum points obtained from the measurements.

At those points, we can estimate the fluctuation amplitude. The fluctuation difference in these maximum and minimum points can be expressed as

$$\Gamma_{\text{diff}} = \cos^{-1}\left(\frac{\sin a}{a}\right) \tag{10}$$

Using Eq. (10) and the calculated retardance, for the maximum and minimum points, we obtain $\Gamma_{\text{diff}}$. Then, we estimate the fluctuation amplitude, and, eventually, we can correct the measurements of the retardance using the exact Eq. (9) instead of the classical one (Eq. (1)) [10].

### 2.2. Applying the method to a PA-LCoS microdisplay

To validate and test the method described in the previous section, we use the next experimental setup.

**Figure 4** shows the experimental setup used to measure the average retardance versus the applied voltage (gray level) for a PA-LCoS device. It consists of a light source (He-Ne laser, $\lambda = 633$ nm), the LCoS, the necessary input and output linear polarizers which are in parallel or crossed configuration, and a radiometer to measure the intensity. For measuring time variations in the retardance, we need to measure the intensity in both cases (parallel and crossed) at the same time, for this reason we have introduced two high-quality nonpolarizing cube beam splitters (model 10BC16NP.4, from Newport): one of them to separate the incident and the reflected beams, and the other to enable synchronized measurement of the parallel and crossed intensities.

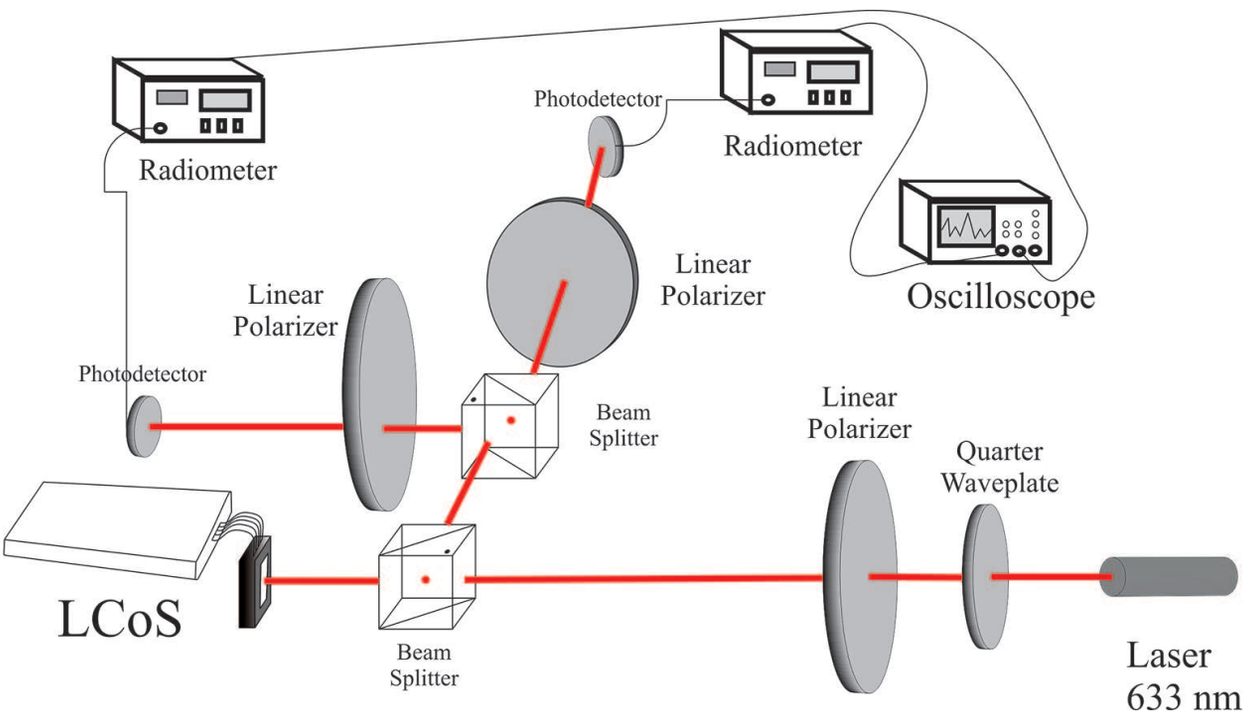


**Figure 4.** Experimental setup used to measure the linear retardance as a function of the applied voltage (gray level) for a PA-LCoS. The setup allows to measure both average and instantaneous values.

These simultaneous measurements when obtained with the help of an oscilloscope are used to validate the estimated fluctuation amplitude calculated with the previous method.

http://dx.doi.org/10.5772/67158

We demonstrated that the estimated values are in good agreement with the measurements done with the oscilloscope [10]. So, the oscilloscope is no longer necessary. This is the reason why we affirm that the method does not need special equipment (as the mentioned oscilloscope), which maybe is not found in an optical laboratory.

In our experiments, we have used and analyzed an LCoS display distributed by the company HOLOEYE. It is an active matrix reflective mode device with 1920 × 1080 pixels and 0.7" diagonal named PLUTO spatial light modulator. The pixel pitch is of 8.0 μm and the display has a fill factor of 87%. The signal is addressed via a standard digital visual interface (DVI) signal. Using an RS-232 interface and its provided software, we can perform gamma control to configure the modulator for different applications and wavelengths. The manufacturer provides some configuration files for the equipment. These configurations are designed for different applications. The configuration files are labeled as "18-6 default," "18-6 2pi linear 633 nm," and "5-5 2pi linear 633 nm." From the name, we can infer that the ones with "2pi linear 633 nm" are designed for a linear response in retardance for 633-nm wavelength. The labeled as "default" means that no gamma correction has been applied and the retardance response will be nonlinear. The other part of the label (18-6 and 5-5) makes reference to the configuration of the digital addressed signal. This part reflects the number of bits used in the signal, so the signal has different lengths depending on the configuration file. In principle, a shorter length presents less flicker. You can find more information about the digital signal and configuration in Refs. [10, 11].

The method presented in Section 2.1 enables us to correct the measures done for characterizing the PA-LCoS in order to know the exact average retardance introduced by each gray level. To do that, we extrapolate the fluctuation amplitude value calculated from the extremals (180° multi ples) to a wider gray level range: the fluctuation amplitude value from the first extremal is consi dered to be roughly valid until half of the gray level distance between itself and the next extremal.

In **Figure 5**, we show the directly taken measurements ("Uncorrected" ones) that we obtain by applying Eq. (1) to the parallel and crossed intensities measured. We know that we are not taking into account the presence of fluctuations. From the extremal points, which are multiples of 180° in the retardance, we can calculate the fluctuation amplitude using Eq. (11). In this way, we obtain a fluctuation amplitude that we apply by intervals between the different extremals. Using Eq. (9), and knowing the value of the fluctuation, we recalculate the average retardance correcting the previous obtained curves ("Corrected" ones).

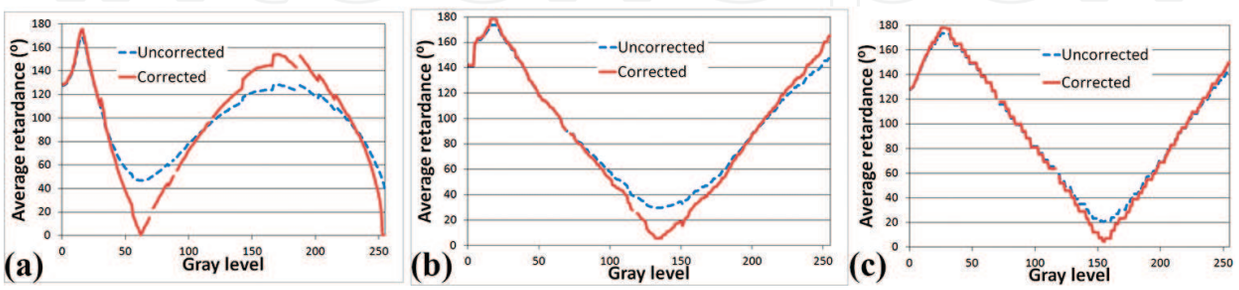


**Figure 5.** Average retardance versus gray level considering the existence of the fluctuation amplitude in the retardance, "corrected" curve, and considering the ideal $a = 0°$, "uncorrected" curve. (a) "18-6 default"; (b) "18-6 2pi linear 633 nm"; (c) "5-5 2pi linear 633 nm".

To sum up: we are able of obtain the corrected curves. With this information, we can change the gamma curve configuration to obtain a selected behavior. And we can just evaluate $\Gamma_{diff}$ in the extremals to select the configuration that has less fluctuation amplitude [10, 12].

### 2.3. Characterization using averaged stokes polarimetry

The method showed in the previous section enables us to configure the device but it does not provide a full characterization. We only have information about the fluctuation amplitude in some points. In this section, we present a method that provides full information about the average retardance and the fluctuation amplitude for all gray levels.

We will use the Mueller-Stokes formalism [8], which enables to deal both with polarized and with unpolarized light. In this formalism, the retardance wave plate matrix is

$$M_R(\Gamma) = \begin{pmatrix} 1 & 0 & 0 & 0 \\ 0 & 1 & 0 & 0 \\ 0 & 0 & \cos\Gamma & \sin\Gamma \\ 0 & 0 & -\sin\Gamma & \cos\Gamma \end{pmatrix} \tag{11}$$

Eq. (11) describes a wave plate with the fast axis along the $X$-axis and a retardance $\Gamma$. Let us consider a unit intensity Stokes vector corresponding to a state of polarization linearly polarized at +45° with respect to the $X$-axis impinging perpendicular onto the linear retarder. Then, the SOP at the exit is calculated as follows:

$$\begin{pmatrix} 1 \\ 0 \\ \cos\Gamma \\ -\sin\Gamma \end{pmatrix} = \begin{pmatrix} 1 & 0 & 0 & 0 \\ 0 & 1 & 0 & 0 \\ 0 & 0 & \cos\Gamma & \sin\Gamma \\ 0 & 0 & -\sin\Gamma & \cos\Gamma \end{pmatrix} \begin{pmatrix} 1 \\ 0 \\ 1 \\ 0 \end{pmatrix} \tag{12}$$

In Eq. (12), we see how the second element of the resultant Stokes vector is zero independently of the retardance introduced by the wave plate, and it does not depend on the possible temporal retardance fluctuations. If we introduce the signal variation model described in Eq. (4), we calculate the average value for $S_2$ and $S_3$ components as follows:

$$\langle S_2 \rangle = \frac{1}{T/2} \int_0^{T/2} \cos\left(\overline{\Gamma} - a + \frac{2a}{T/2}\, t\right) dt = \frac{\sin(a)}{a} \cos(\overline{\Gamma}) \tag{13}$$

$$\langle S_3 \rangle = \frac{-1}{T/2} \int_0^{T/2} \sin\left(\overline{\Gamma} - a + \frac{2a}{T/2}\, t\right) dt = \frac{-\sin(a)}{a} \sin(\overline{\Gamma}) \tag{14}$$

Therefore, the average exit vector $S_{out}$ reflected by the PA-LCoS when a linear polarized beam impinges, and the angle between the slow axis and the polarizer is 45° is given by

$$\langle S_{out} \rangle = < \begin{pmatrix} 1 \\ 0 \\ \cos\Gamma(t) \\ -\sin\Gamma(t) \end{pmatrix} > = \begin{pmatrix} 1 \\ 0 \\ \frac{\sin(a)}{a} \cos(\overline{\Gamma}) \\ -\frac{\sin(a)}{a} \sin(\overline{\Gamma}) \end{pmatrix} \tag{15}$$

http://dx.doi.org/10.5772/67158

From Eq. (15), we see how, when we calculate the degree of polarization (DoP), it depends only on the fluctuation amplitude

$$\mathrm{DoP} = \frac{\sqrt{\langle S_1\rangle^2 + \langle S_2\rangle^2 + \langle S_3\rangle^2}}{S_0} = \frac{\sin(a)}{a} \tag{16}$$

Eq. (16) shows that the DoP is produced by the fluctuation in the retardance and provides as a way to calculate the fluctuation amplitude for every gray level by measuring the DoP.

From Eq. (15), it is clear that the average retardance can be obtained by calculating the ration between third and fourth Stoke vector components,

$$-\langle S_3\rangle / \langle S_2\rangle = tg(\overline{\Gamma}) \tag{17}$$

We have presented a method that can be applied to any electro-optic element acting as a wave plate and presenting fluctuations in its optical response [10]. It is not only applicable to PA-LCoS devices. We have applied them to the mentioned PLUTO device obtaining a complete characterization [13].

*2.3.1. Experimental setup for characterization*

To use the method described above, we just need a polarimeter. In our case, we have used a commercial PAX5710VIS-T model from THORLABS. This is a rotating wave plate-based polarimeter, which belongs to time-division mode polarimeters. They are not able to provide instantaneous values if the state of polarization changes more rapidly than its measurement time interval. In our case, the THORLABS polarimeter has a measurement time interval of 3 ms (maximum rotation frequency is 333 Hz). But as long as we need an average value, and the software allows to enlarge the measurement time interval, we just select an appropriate time interval larger than the fluctuation time period of the PLUTO device, which is about 8.66 ms (120 Hz).

In **Figure 6**, we show the experimental setup used for characterizing our PA-LCoS, the first wave plate shown is used just to guarantee enough light intensity regardless of the polarizer angle, since the output light from the laser is linearly polarized. A quarter wave plate, as in the figure, with its neutral lines properly oriented can do the work, even though it is not the only possibility. As we show in the method the input polarizer has to be at 45° from the neutral lines of our PA-LCoS, in our case it is the *x*-*y*-axis.

We test the method with the "18-6 633 nm 2pi linear" and "5-5 633 nm 2pi linear" configurations, already introduced. We measure the Stokes vector and degree of polarization of each gray level. We have obtained the next results.

**Figure 7** shows the data obtained for the two different configurations tested when linearly polarized light impinges onto the device at 45°. In dashed lines, we show the measurements for "5-5 633 nm 2pi linear" configuration. In continuous lines, we show the measurements

for "18-6 633 nm 2pi linear." The first thing that we have to note is that parameter $S_1$ is close to zero for all gray levels, in clear confirmation of the result obtained in Eq. (15). To obtain the retardance value and the fluctuation amplitude, we have to apply Eqs. (17) and (16), respectively.

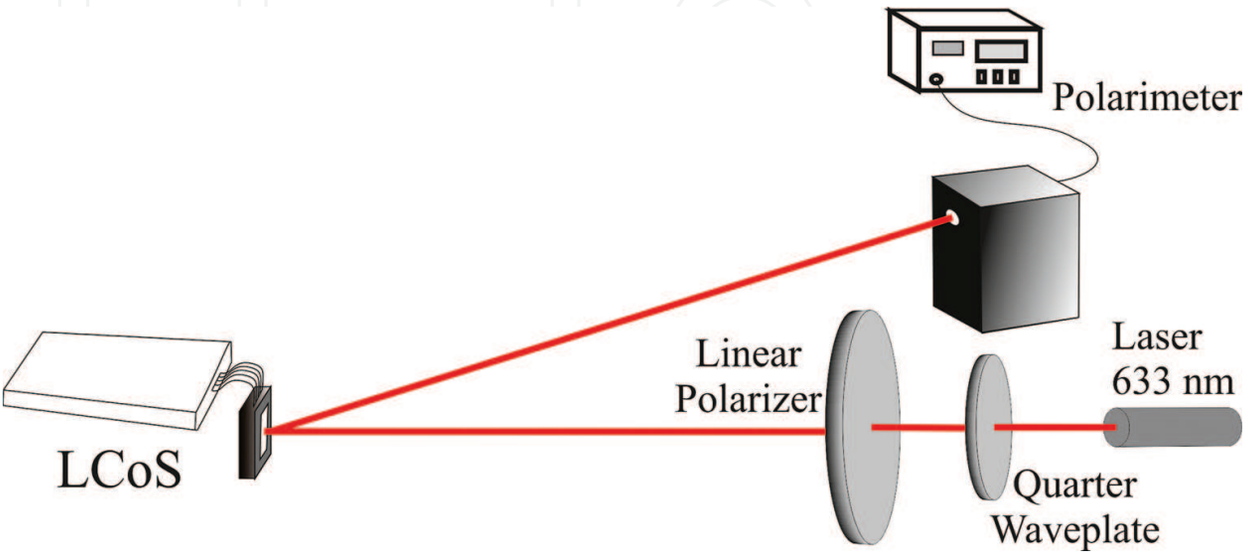


**Figure 6.** Experimental setup for characterizing a PA-LCoS.

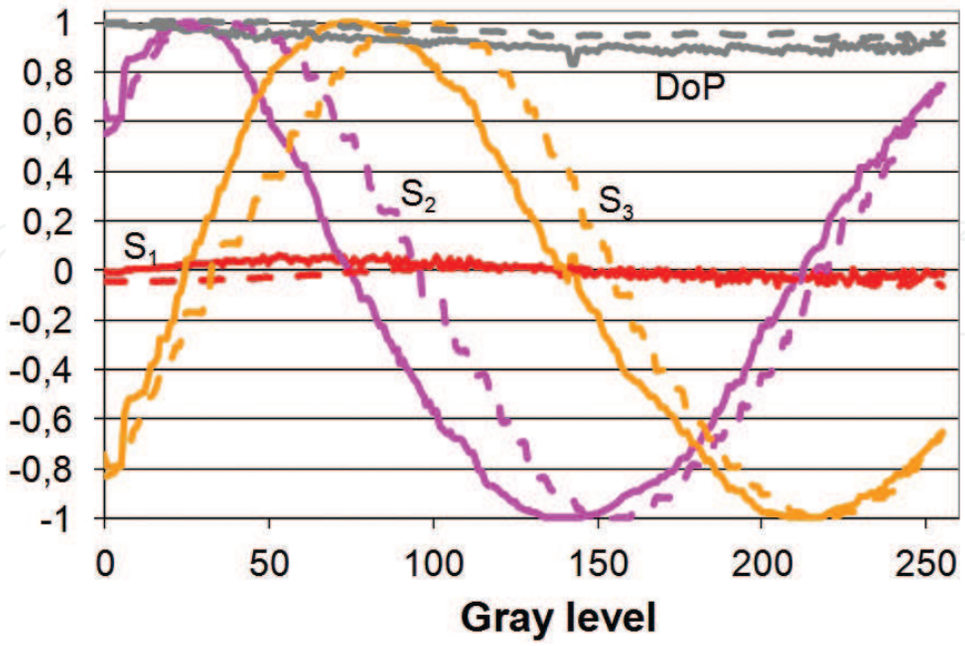


**Figure 7.** Measurements obtained from the PLUTO for "5-5 633 nm 2pi linear" (dashed line) and "18-6 633 nm 2pi linear" (continuous line).

http://dx.doi.org/10.5772/67158

In **Figure 8**, we have calculated the fluctuation amplitude and the average retardance. We have obtained a full characterization of the device. We observe that the retardance range is about 360° for both sequences with very good linearity. The fluctuation amplitude is clearly smaller for the 5-5 sequence.

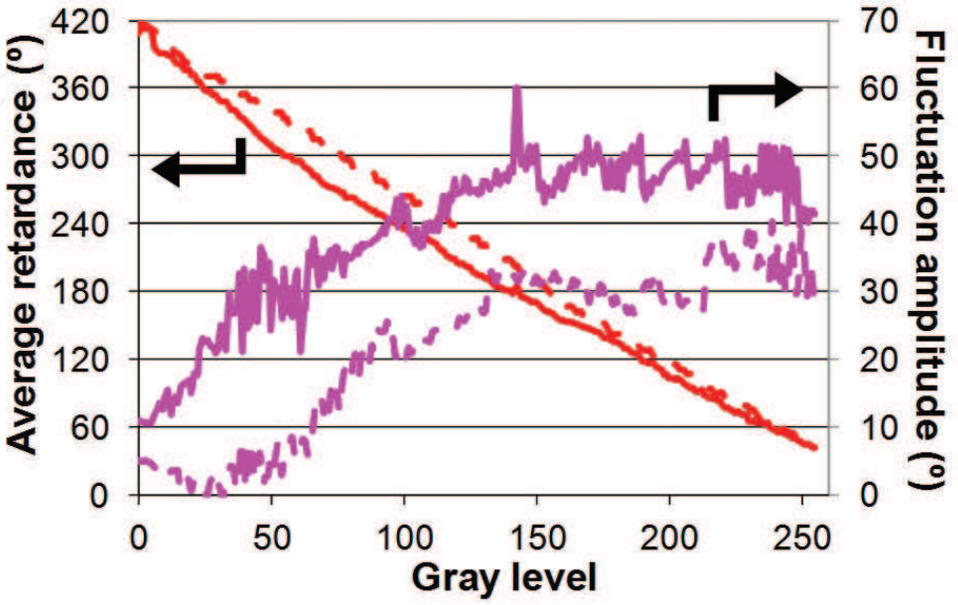


**Figure 8.** Calculated values for the average retardance and the fluctuation amplitude for $\lambda$ = 633 nm, and for sequences "5-5 633 nm 2pi linear" (dashed) and "18-6 633 nm 2pi linear" (continuous).

This method has been validated with the direct measurements of the retardance fluctuations and with the predictive capability of the SOP at the exit regardless of the SOP at the input [13]. The direct measurements of the fluctuation amplitude have been done with the help of an oscilloscope [14], and we have also tested the predictive capability of the model when applied to a more complex diffractive optical element (DOE) as a blazed grating [15].

## 3. Using a PA-LCoS in a holographic data storage system

We have a good characterization method and control over the display that will act as a spatial light modulator in our holographic data storage system. We present how we can implement different modulation schemes with a phase-only device as our PA-LCoS.

HDSS enables true three-dimensional (3-D) storage of information and also associative memory retrieval [16]. There are many aspects that need to be addressed for HDSS to be commercially viable [2]. These systems are always taking advantage from the latest technological advances in the various components that form a complete system. In this sense, PA-LCoS microdisplays have replaced previous liquid-crystal display (LCD) technology in most photonics applications [17]; this fact makes PA-LCoS an interesting device to test in

HDSS. PA-LCoS are high-resolution reflective devices which enable phase-only operation. They are ideal for binary or multinary phase-only data pages [18, 19]. This leads to DC term cancellation when recording the Fourier transform of the data page, avoiding the premature saturation of the recording material.

### 3.1. Modulation schemes

We try to implement the well-known binary intensity modulation (BIM) and the hybrid ternary modulation (HTM) [20, 21]. PA-LCoS devices are designed for displaying phase-only elements without coupled amplitude. This is easily achieved by illuminating them with a linearly polarized light parallel to the director axis. We have investigated that the PA-LCoS can also be used to display the widely applied BIM data pages. We also try to implement the more demanding HTM data pages. HTM had not been studied with PA-LCoS devices. HTM has the advantage that combines the ease of detection of BIM data pages (that only needs to detect intensity) and it reduces the DC term of the Fourier transform. The reduction on the DC term is necessary to avoid saturation of the dynamic range of the recording material [20, 21].

We use the model and characterization technique presented in Section 2.3 that enable us to obtain the average retardance and fluctuation amplitude for every gray level. Before applying the configuration needed, we need to calculate the complex amplitude of the electric field at the exit. To do that, we use the Jones matrix formalism, so we present the basic elements involved,

$$P_X = \begin{pmatrix} 1 & 0 \\ 0 & 0 \end{pmatrix} \tag{18}$$

Eq. (18) is the matrix associated to a linear polarizer with its transmission axis along the *X*-axis,

$$W(\phi) = \begin{pmatrix} \exp(-j\phi/2) & 0 \\ 0 & \exp(+j\phi/2) \end{pmatrix} \tag{19}$$

Eq. (19) is the matrix for a linear retarder of linear retardance $\varphi$ with its slow axis along the *X*-axis. When polarization elements are rotated an angle $\theta$ with respect to the *X*-axis, we need the two-dimensional rotation matrix,

$$R(\theta) = \begin{pmatrix} \cos\theta & \sin\theta \\ -\sin\theta & \cos\theta \end{pmatrix} \tag{20}$$

To produce both BIM and HTM with the PA-LCoS device, we need to insert the display between two rotated linear polarizers at angles $\theta_1$ and $\theta_2$, that is, the complex amplitude for the electric field at the output is given by the following equation:

$$\vec{E}_{OUT} = P_X \cdot R(\theta_2) \cdot W_{PA}(\overline{\Gamma}) \cdot \begin{pmatrix} \cos\theta_1 \\ \sin\theta_1 \end{pmatrix} \tag{21}$$

http://dx.doi.org/10.5772/67158

where $\vec{E}_{OUT}$ corresponds to linearly polarized light at an angle $\theta_2$, always with respect to the $X$-axis. $W_{PA}(\bar{\Gamma})$ is the matrix for the PA-LCoS which is given by Eq. (19), and whose average retardance varies with gray level, and it will be given by our characterization method. Its fluctuation amplitude will not be considered in the calculations: in the calibration we have taken care to select electrical configurations minimizing the existence of this flicker in the retardance [9, 10].

If we take into account the calculated values for the average retardance, we can calculate the trajectories in the complex plane. In **Figure 9**, we present the configurations used to implement the different modulation schemes.

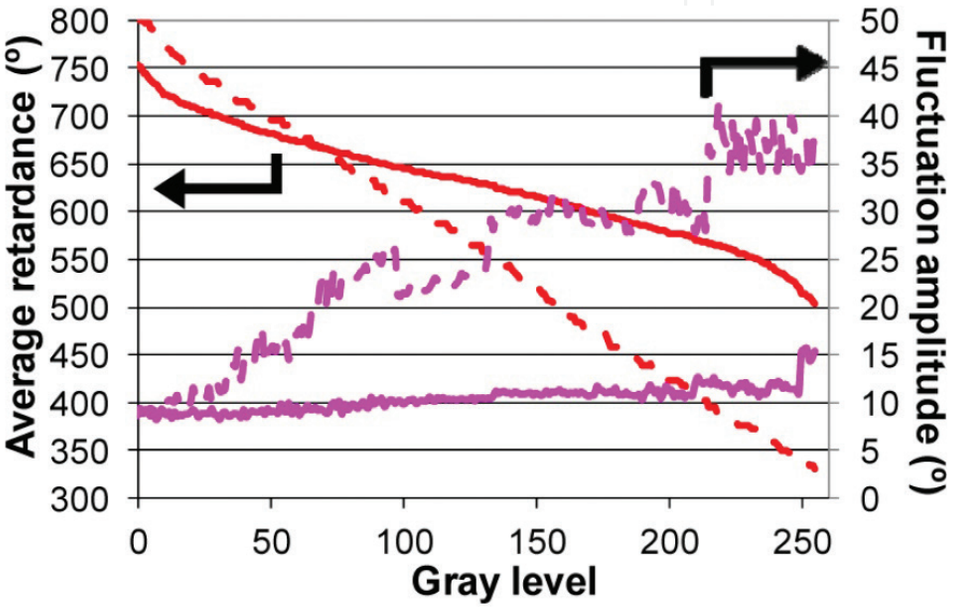


**Figure 9.** Calculated values of the average retardance and the fluctuation amplitude for $\lambda$ = 532 nm at an angle of incidence of 11.5°, for two different device configurations that enables us to implement BIM (continuous) and HTM (dashed).

The configuration shown in **Figure 9** is obtained at an angle of incidence of 11.5°, which is the incidence angle presented in our setup for holographic data storage. The sequences used are both 5-5, but the voltages applied are changed for the BIM configuration (continuous lines in **Figure 9**). In this case, the voltage has been reduced to $V_{bright}$ = 2.02 V and $V_{dark}$ = 1.11 V. For BIM, we only need a phase depth of 180°, this is the reason that we can relax the requisites of the device. As shown in **Figure 9**, the fluctuation amplitude has been reduced, in comparison with the configuration used for HTM that is the configuration called "5-5 532 nm 2pi linear" provided by the manufacturer. For more information about the influence of $V_{bright}$ and $V_{dark}$, reference [12] can be consulted.

After we have defined the average retardance, from Eq. (21) we can calculate the intensity transmission $I_{OUT}$ that is given by the hermitic product of $\vec{E}_{OUT}$ and the phase shift $\varphi_{OUT}$ will be given by the argument. We can optimize in the computer the angles $\theta_1$ and $\theta_2$ of the linear polarizers to produce the best BIM and HTM regimes.

In the case of BIM, we need to generate the maximum intensity contrast between the on and off values, that is, $I_{contrast} = I_{oOn}/I_{Ooff}$. We need at least a contrast of 1:20 for achieving an acceptable bit error rate (BER) [22]. Maximum contrast can be obtained with only polarizers, if they are parallel of crossed with each other at 45° with respect to the director axis of the PA-LCoS. Using the data from **Figure 9**, we obtain the intensity transmission and phase-shift curves as a function of the gray level. It is displayed in **Figure 10(a)**, which are also represented as a phasor in the complex plane in **Figure 10(b)**

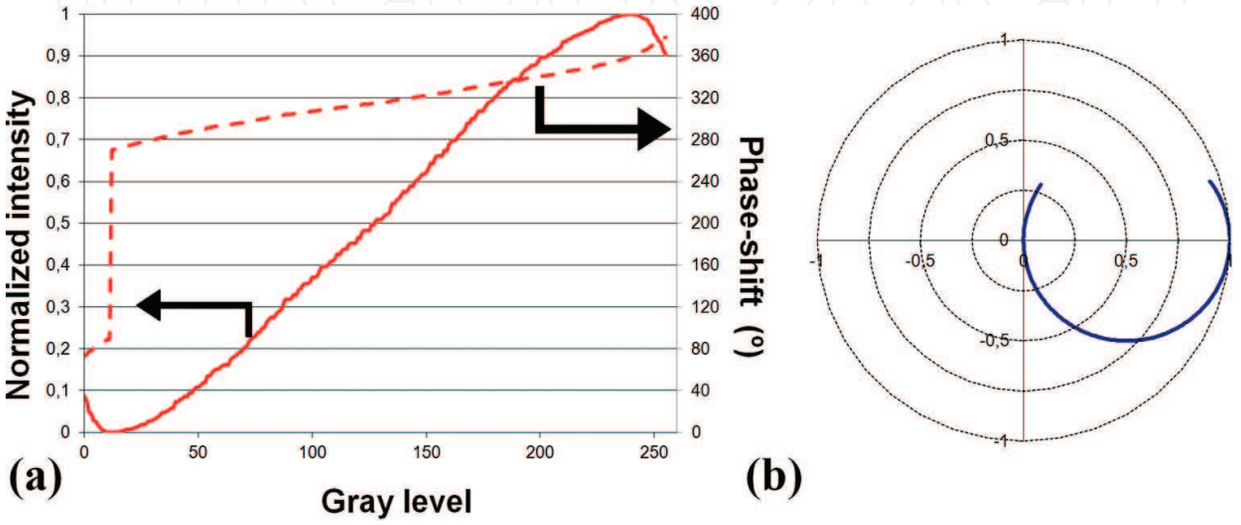


**Figure 10.** Simulation for BIM. (a) Intensity transmission and phase shift as a function of gray level; (b) phasor evolution in the complex plane. The PA-LCoS is sandwiched between linear polarizers at +45° with respect to the *X*-axis (neutral lines).

In **Figure 10(a)**, the lowest and highest intensity transmission points occur at gray levels 12 and 239, respectively. From the values, we calculate that the theoretical contrast tends to infinity, and the phase-shift values are 270° and 360°. From **Figure 9**, we see that the difference in the retardance value is very close to 180° between these two gray levels. In the experimental measurements, we obtain that the low and high transmission points occur slightly displaced at gray levels 14 and 248, and the contrast we measure is about 1:50. The theoretical contrast value is idealistic since the various degradation effects in the PA-LCoS have a direct impact on the minimum intensity.

The representation in the complex plane (**Figure 10(b)**) is useful to see the complex evolution and the trajectory described with the variation of gray level. We see that the 180° phase jump is produced at the vicinity of the origin (gray level 12). It can be verified that independently of the orientation of the transmission axis of the polarizers, we always obtain a circular trajectory. The same effect is produced when adding wave plates to the system, at the entrance or/and the exit of the PA-LCoS (it will be like adding an offset to the retardance; it will not vary the trajectory). This will be a problem when implementing the HTM scheme.

http://dx.doi.org/10.5772/67158

For HTM scheme, we need three gray level values, two of them with a 180° relative phase shift and an equal and high intensity level (On levels). The third level will be the Off level that has to block as much light as possible to obtain a good contrast. As long as the trajectories in the complex plane are always circular and the 180° phase jump is produced in the origin, we have found that the PA-LCoS device cannot fully meet these requirements. In the case of Twisted-Nematic (TN) LCDs, this is possible. TN LCDs provided a coupled amplitude and phase-shift modulation. This fact enables to produce arbitrary complex amplitude trajectories that can accomplish the requirements of HTM [20, 21].

Therefore, we can produce a compromise solution by slightly shifting the circular trajectory. At the cost of leaking some light intensity in the Off level, we can achieve two On levels with an appreciable transmitted intensity and a relative phase shift close to 180°. The closer these On levels are to a phase difference of 180° the lower the DC term is. We have named this modulation scheme as pseudo-HTM modulation (p-HTM). We want to know if this p-HTM scheme is still useful for its application in an HDSS.

In **Figure 11**, we show the complex amplitude for one of the possible p-HTM configurations. It corresponds to input and output polarizers at 55° and −45° with respect to the slow axis. In **Figure 11(a)**, we show the intensity and the phase-shift versus gray level, and in **Figure 11(b)** we plot the phasor evolution in the complex plane where we see that the circular trajectory is slightly displaced from the origin. The two On gray levels considered are 105 and 168 with amplitude transmission values of 0.28 and phase-shift difference of 206°. The Off gray level is 140 with an amplitude transmission of 0.03 and phase shift 170°. The intensity contrast is then 1:10. This is a low value; however, increasing the contrast means almost crossing the two polarizers. This produces that the 180° phase jump is closer to the origin and the difference in phase between On levels is increased rapidly producing a larger DC term, which is what we are trying to reduce [23].

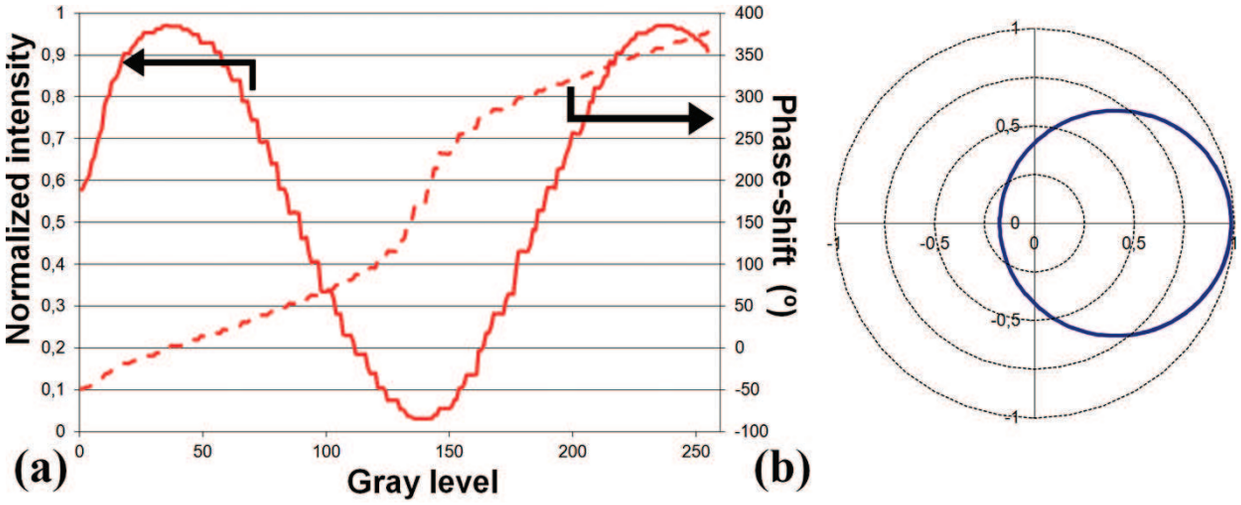


**Figure 11.** Simulation for p-HTM: (a) intensity transmission and phase shift; (b) phasor evolution in the complex plane. input and output polarizers are at +55° and −45° with respect to the slow axis.

### 3.2. Experimental results

To test the modulation schemes presented, we use the next experimental setup represented in **Figure 12**.

**Figure 12** shows us the scheme for the experimental HDSS used. We consider a 532-nm laser beam, to which the PVA photopolymer is sensitized. We use PVA/AA because it is a well-studied photopolymer, and our group had done an intense work to characterize and model it. More information about the photopolymer can be found in references [24, 25]. We have inserted a half wave plate before the shutter and spatial filter to ensure that enough light intensity impinges onto the linear polarizers in the object and reference beam. The intensity ratio between both beams is controlled with one attenuator in reference beam. The linear polarizers LP are used to produce the appropriate SOP for the object and reference beam. In the reference beam, a stop limits the aperture of the beam to about a diameter of 1 cm. Lenses in the reference beam form an afocal system so that the rotating mirror and the recording material are at conjugate planes; this enables angular multiplexing simply by rotation of the mirror. In the object beam, we have combined a divergent and a convergent lens in order to control the curvature of the converging beam onto the PA-LCoS. At the convergence plane, we find the Fourier transform of the data page, in this plane we used a stop that will act as a Nyquist filter. Then we have built a relay system to image the Nyquist filter plane onto the recording plane. We can also introduce some defocusing degree by displacing the recording material plane. This system uses a convergent correlator setup, and finally we read the data saved with the help of a high dynamic CCD camera [25].

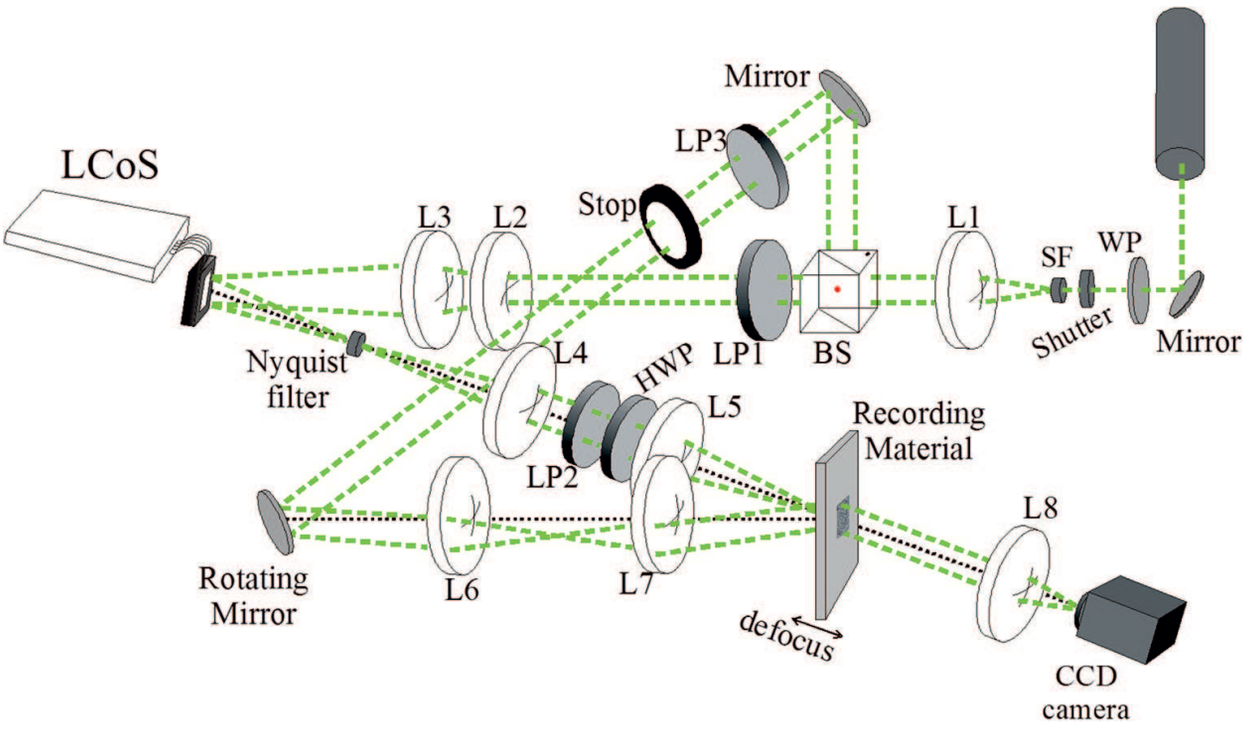


**Figure 12.** Schematic representation of our experimental HDSS testing platform.

http://dx.doi.org/10.5772/67158

In the present work, we focus on testing the modulation schemes implemented with our PA-LCoS. We address a data page formed with random data bits. Afterwards, in the reconstruction step, we retrieve the data saved with CCD camera. Compared with the original data, we make a count on the errors detected. This provides us with a measurement or the raw BER. We only apply a simple treatment consisting in looking for the best threshold level that minimizes the errors counted [26].

The data page is formed by 64 × 64 information bits, and each bit of information is formed by 8 × 8 pixels in the PA-LCoS. This is necessary to avoid interpixel cross-talk effects [16]. We have 4096 information bits of information in each data page.

In **Figure 13**, we present the first result for BIM scheme; in this case, we are not using material to register the hologram. This image enables us to evaluate the optics performance of our experimental setup (**Figure 12**). We see some interesting facts. In the first place, we see how the data page is perfectly reconstructed and the 1's and 0's distribution in gray levels is clearly separated. No errors in the reconstruction have been produced.

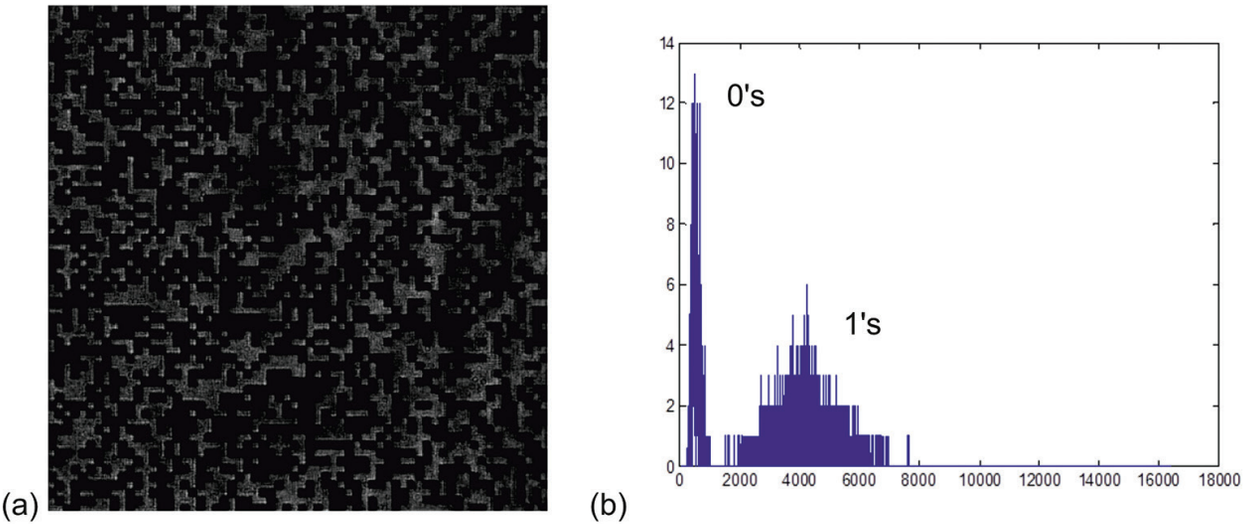


**Figure 13.** Experimental results for BIM scheme and no material. (a) Data page; (b) histograms.

In **Figure 14**, we present the results obtained for p-HTM scheme without using material. We see that the histograms are not clearly separated. This implies that some error will be produced in the reconstruction. We detect eight errors, which corresponds to a BER of $2.0 \times 10^{-3}$. This is due to the lower contrast of the data page, but we still can reconstruct the image with an acceptable BER.

**Figure 15** shows us the results obtained when the data page is stored in a PVA/AA film. The beam intensity ratio used is about 1:400, where the intensity incident onto the recording material is 3.16 mW/cm$^2$ and 8 μW/cm$^2$, respectively, for the reference and object beam, and for an exposure time of 6 s. As we can see in the histograms, the 0's and 1's show a slight overlap. We detected 52 errors, that is, BER = $1.3 \times 10^{-2}$. The BER is still in the range that allow to retrieve the information without errors when applying error correction codes [26].

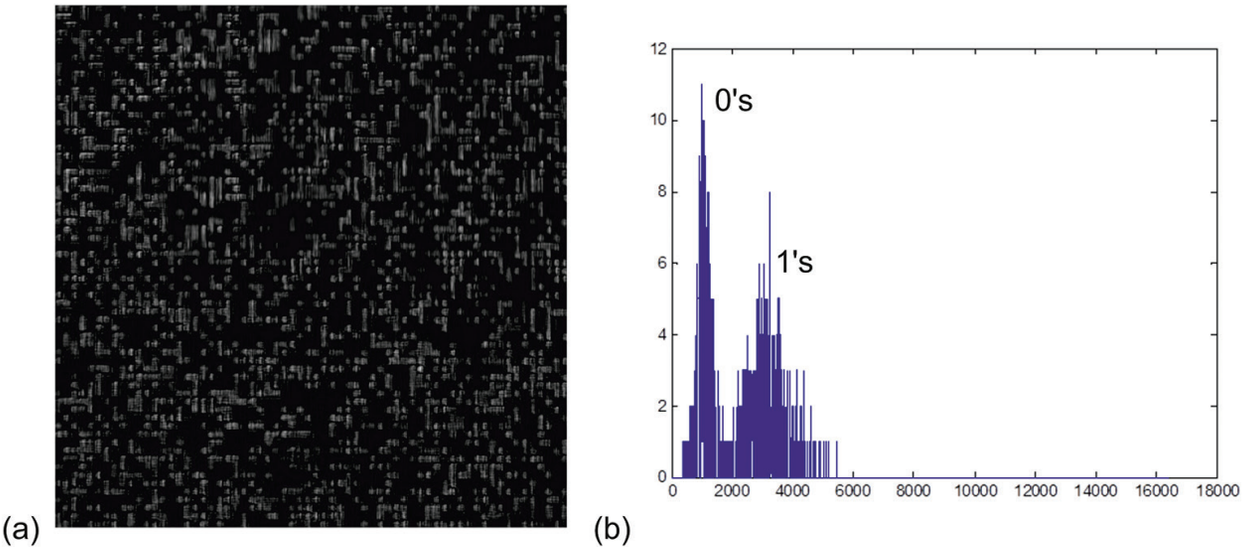


**Figure 14.** Experimental results for p-HTM scheme and no material. (a) Data page; (b) histograms.

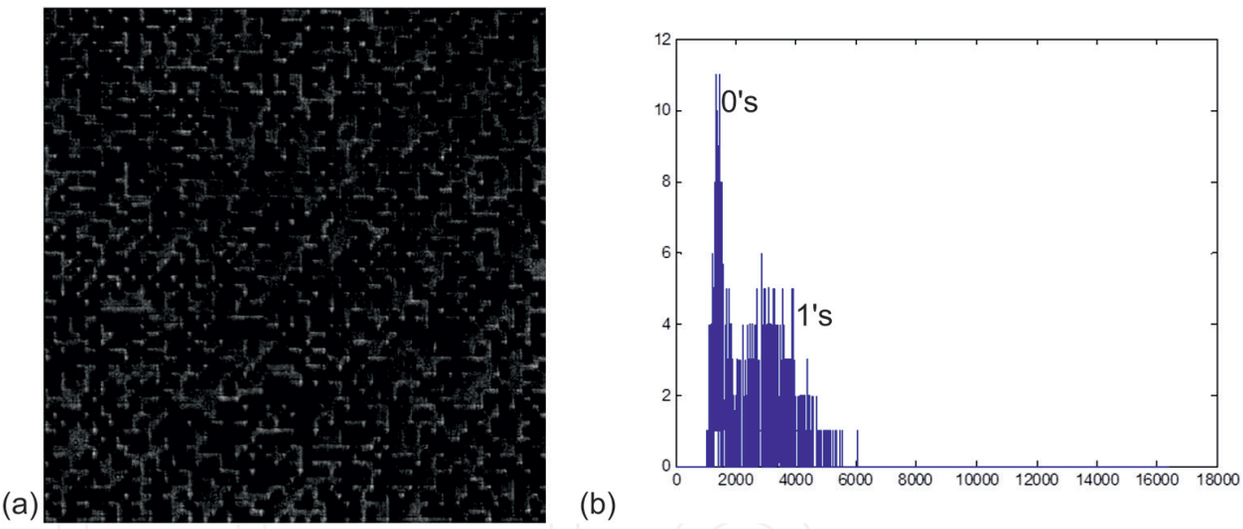


**Figure 15.** Experimental results for BIM scheme and PVA/AA. (a) Data page; (b) histograms.

In **Figure 16**, we see the results for a data page stored in PVA/AA using p-HTM scheme. Beam intensity ratio is about 1:800, where the intensity incident onto the recording material is 3.16 mW/cm$^2$ and 4 μW/cm$^2$, respectively, for the reference and object beam, and for an exposure time of 10 s. As we can see, and due to the lost of contrast, the results are a worse that in BIM case. There are 229 errors detected, that is, BER = $5.6 \times 10^{-2}$. BER is still in an acceptable range, and it is only five times larger than the BIM case.

We did some simulations to predict the results [23]. Our simulations predicted worse results for p-HTM, when we compare it with BIM, than the ones obtained experimentally. We believe that the better experimental ratio is due to the reduction in DC term, which is to not have into account in our simulations just because we considered a linear material. Further experimental

http://dx.doi.org/10.5772/67158

work has to be done with PVA/AA photopolymer to study these saturation effects. In general, we can say that the p-HTM scheme can be used in an HDSS because of its promising results. Maybe, it can show all its potential when the multiplexing capability will be used.

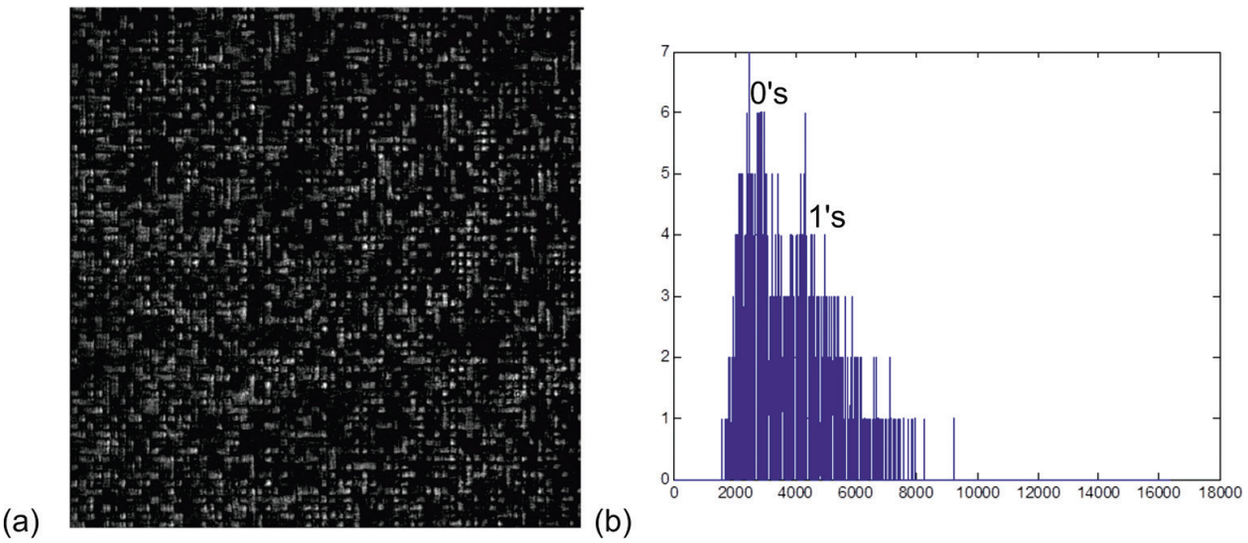


**Figure 16.** Experimental results for p-HTM scheme and PVA/AA. (a) Data page; (b) histograms.

## 4. Conclusions

This chapter presents how to apply a novel PA-LCoS microdisplay to an HDSS. To accomplish that, we presented two methods to characterize the device. The first method does not use any special equipment and permits us to customize the configuration of the PA-LCoS. The second one enables a complete characterization and presents a good prediction capability, which will be useful to test if the device can be applied in a specific setup or application. The method has been validated in different ways, and can be applied to any device that acts as a wave plate but present some fluctuation in the introduced retardance.

When we have characterized the PA-LCoS microdisplays, we have applied it in a complete HDSS. We have found that we can design some modulation schemes that can be used in HDSS. We present the promising p-HTM scheme that can be comparable with the widely used BIM scheme in terms of BER.

## Acknowledgements

We want to acknowledge the financial support from the Spanish Ministerio de Trabajo y Competitividad under projects FIS2014-56100-C2-1-P and FIS2015-66570-P and by the Generalitat Valenciana of Spain under projects PROMETEOII/2015/015 and ISIC/2012/013 and by the University of Alicante with the project GRE12-14.

## Author details

Francisco J. Martínez Guardiola*, Andrés Márquez Ruiz, Sergi Gallego Rico, Roberto Fernández Fernández, Jorge Francés Monllor, Manuel Ortuño Sánchez, Inmaculada Pascual Villalobos and Augusto Beléndez Vázquez

*Address all correspondence to: fj.martinez@ua.es

Instituto de Física Aplicada a las Ciencias y las Tecnologías, Universidad de Alicante, Alacant, Spain

## References

[1] J. Turunen and F. Wyrowski, editors. Diffractive Optics for Industrial and Commercial Applications. Berlin: Akademie Verlag; 1997.

[2] H. J. Coufal, D. Psaltis, and B. T. Sincerbox, editors. Holographic Data Storage. Springer-Verlag ed. Berlin: Springer-Verlag; 2000.

[3] G. Lazarev, A. Hermerschmidt, S. Krüger, S. Osten. LCOS Spatial Light Modulators: Trends and Applications. in Optical Imaging and Metrology: Advanced Technologies: John Wiley & Sons; 2012.

[4] Z. Zhang, Z. You, D. Chu. Fundamentals of phase-only liquid crystal on silicon (LCoS) devices. Light Sci. Appl. 2014; **3**:1–10. DOI: 10.1038/lsa.2014.94

[5] S. T. Wu and D. K. Yang. Reflective Liquid Crystal Displays. Chichester: John Wiley & Sons Inc.; 2005.

[6] A. Lizana et al. Influence of the temporal fluctuations phenomena on the ECB LCoS performance. In: SPIE, editor. Proceeding of SPIE; 2012; EEUU: SPIE; 2012. p. 74420G.

[7] J. García-Márquez, V. López, A. González-Vega, E. Noé. Flicker minimization in a LCoS spatial light modulator. Opt. Express. 2012;**20**:8431–8441. DOI: 10.1364/OE.20.008431

[8] G. Goldstein. Polarized Light. New York, NY: Marcel Dekker; 2003.

[9] P. A. Williams, A. H. Rose, and C. M. Wang. Rotating-polarizer polarimeter for accurate retardance measurement. Appl. Optics. 1997;**36**:6466–6472.

[10] F. J. Martínez, A. Márquez, S. Gallego, J. Francés, I. Pascual. Extended linear polarimeter to measure retardance and flicker: application to liquid cystal on silicon devices in two working geometries. Opt. Eng. 2014;**53**(1):014105-1– 014105-9. DOI: http://dx.doi.org/10.1117/1.OE.53.1.014105

[11] A. Hermerschmidt, S. Osten, S. Krüger and T. Blümel. Wave front generation using a phase-only modulating liquid-crystal based micro-display with HDTV resolution. In: SPIE, editor. Proceedings of SPIE; 2007; EE.UU.: SPIE; 2007. p. 65840E.

[12] F. J. Martínez, A. Márquez, S. Gallego, M. Ortuño, J. Francés, A. Beléndez and I. Pascual. Electrical dependencies of optical modulation capabilities in digitally addressed parallel aligned liquid crystal on silicon devices. Opt. Eng. 2014;**53**(6):067104. DOI: http://dx.doi.org/10.1117/1.OE.53.6.067104

[13] F. J. Martínez, A. Márquez, S. Gallego, J. Francés, I. Pascual and A. Beléndez. Retardance and flicker modelling and characterization of electro-optic linear retarders by averaged Stokes polarimetry. Opt. Lett. 2014;**39**:1011–1014. DOI: http://dx.doi.org/10.1364/OL.39.001011

[14] F.J. Martínez, A. Márquez, S. Gallego, M. Ortuño, J. Francés, A. Beléndez and I. Pascual. Averaged Stokes polarimetry applied to evaluate retardance and flicker in PA-LCoS devices. Optics Express. 2014;**22**:15064–15074. DOI: http://dx.doi.org/10.1364/OE.22.015064

[15] F. J. Martínez, A. Márquez, S. Gallego, M. Ortuño, J. Francés, I. Pascual and A. Beléndez. Predictive capability of average Stokes polarimetry for simulation of phase multilevel elements onto LCoS devices. Appl. Optics. 2015;**54**(6):1379–1386. DOI: http://dx.doi.org/10.1364/AO.54.001379

[16] D. Sarid and B.H. Schechtman. A roadmap for data storage applications. Opt. Photonics News. 2007;**18**(5):32–37. DOI: https://doi.org/10.1364/OPN.18.5.000032

[17] G. Lazarev, A. hermerschmidt, S. Krüger and S. Osten. LCOS spatial light modulator: trends and applications. In: W. Osten and N. Reingand, editors. Optical Imaging and Metrology. Wiley-VCH Verlag GmbH & Co. KGaA; 2012. pp. 1–29. DOI: http://dx.doi.org/10.1002/9783527648443.ch1

[18] J. Joseph and D. A. Waldman. Homogenized Fourier transform holographic data storage using phase spatial light modulators and methods for recovery of data from the phase image. Appl. Optics. 2006;**45**(25):6374–6380. DOI: https://doi.org/10.1364/AO.45.006374

[19] B. Das, J. Joseph and K. Singh. Phase modulated gray-scale data pages for digital holographic data storage. Optics Commun. 2009;**282**(11):2147–2154. DOI: http://dx.doi.org/10.1016/j.optcom.2009.02.048

[20] A. Márquez, S. Gallego, D. Méndez, M. L. Álvarez, E. Fernández, M. Ortuño, C. Neipp, A. Beléndez and I. Pascual. Accurate control of a liquid-crystal display to produce a homogenized Fourier transform for holographic memories. Optics Lett. 2007;**32**(17):2511–2513. DOI: https://doi.org/10.1364/OL.32.002511

[21] E. Fernández, R. Fuentes, A. Márquez, A. Beléndez and I. Pascual. Binary intensity modulation and hybrid ternary modulation applied to multiplexing objects using holographic data storage on a PVA/AA photopolymer. Int. J. Poly. Sci. 2014;**2014**:356534. DOI: http://dx.doi.org/10.1155/2014/356534

[22] M. J. O'Callaghan. Sorting through the lore of phase mask options—performance measures and practical commercial designs. In: SPIE, editor. Advanced Optical and Quantum

Memories and Computing; 17 of June; San Jose, CA, United States. United States: SPIE; 2004. pp. 150–159. DOI: http://dx.doi.org/10.1117/12.529854

[23] F. J. Martínez, R. Fernández, A. Márquez, S. Gallego, M. L. Álvarez, I. Pascual and A. Beléndez. Exploring binary and ternary modulations on a PA-LCoS device for holographic data storage in a PVA/AA photopolymer. Optics Express. 2015;**23:**20459–2047. DOI: https://doi.org/10.1364/OE.23.02045

[24] H. Sherif, I. Naydenova, S. Martin, C. McGinn, V. Toal. Characterization of an acrylamide-based photopolymer for data storage utilizing holographic angular multiplexing. J. Opt. A, Pure Appl. Opt. 2005;**7**:255–260.

[25] C. E. Close, M. R. Gleeson, D. A. Mooney, J. T. Sheridan. Monomer diffusion rates in photopolymer material. Part II. High-frequency gratings and bulk diffusion. J. Opt. Soc. Am. B. 2011;**28**:842–850. DOI: 10.1364/JOSAB.28.000842

[26] Govind P. Agrawal, editor. Fiber-Optic Communication Systems. 4th ed. Rochester, New York, NY: John Wiley & Sons; 2012. 626 p. DOI: 10.1002/9780470918524